 doi:10.20944/preprints201905.0265.v1

Article

Modeling and Simulation of a Novel Piezo-Motor Based on Piezoelectric Properties of $Pb_{(1-x)}Sr_x(Ti_{0,48}Zr_{0,52})_{(1-y)}Nb_yO_3$ Ceramics

Lucian Pîslaru-Dănescu [1, *], Ion Fuiorea [2], Alina Dumitru [3], Lică Flore [4], Albert Arnau Cubillo [5] and Ionel Popescu [6]

[1] Laboratory of Sensors/Actuators and Energy Harvesting, National Institute for Research and Development in Electrical Engineering ICPE-CA, Bucharest 030138, Romania; lucian.pislaru@icpe-ca.ro; Tel.:+40755015611
[2] Associated Professor at Faculty of Aerospace Engineering, University POLITEHNICA, Bucharest 060042, Romania; ifuiorea@yahoo.com
[3] Laboratory of Ceramic Materials, National Institute for Research and Development in Electrical Engineering ICPE-CA, Bucharest 030138, Romania; alina.dumitru@icpe-ca.ro
[4] Defense Systems Department, National Research and Development Institute for Gas Turbines COMOTI, Bucharest 061126, Romania; lica.flore@comoti.ro
[5] Faculty of Aerospace Engineering, University POLITEHNICA, Bucharest 060042, Romania; albert.acubillo@gmail.com
[6] Institute for Theoretical & Experimental Analysis of Aeronautical Structures STRAERO S. A., Bucharest 061126, Romania; ionel.popescu@straero.ro
* Correspondence: lucian.pislaru@icpe-ca.ro

Abstract: First of all the paper presents a solid solution of piezoelectric ceramic that was synthesized according to the general formula $Pb_{(1-x)}Sr_x(Ti_{0.48}Zr_{0.52})_{(1-y)}Nb_yO_3$ with x = 0.05 and y = 0.02, using wet ceramic processing technology and using an oxide mix as prime material. The effects of dopants (Sr^{2+} and Nb^{5+}) on phase constitution, on microstructure and on the dielectric and piezoelectric properties were determinate. The Zr/Ti ratio was chosen near the morphotropic phase boundary of the PZT system in studied composition. The XRD data revealed that the PZT doped composition had tetragonal perovskite structure. Secondly the paper presents the design of the novel piezo-motor based on a surface wave which translates the linear extension of different piezoelectric segments of a piezoelectric cylinder into a rotational bending movement. This rotational bending of the piezoelectric cylinder is then transformed into a continuous rotation of the rotor through a calculated contact. The design of the motor takes advantage of the high piezoelectric constants of the developed material in an optimal way in order to increase the energetic efficiency. A brief mathematical model of electromechanical answer of piezoelectric materials is presented as it was used in the modeling of the material during the numerical simulations.

Keywords: PZT; mixed-oxides techniques; dielectric properties; piezoelectricity; ultrasonic piezo-motor; piezoelectric cylinder; numerical simulation

1. Introduction

The lead zirconate titanate (PZT) with different dopants can be used in different applications for electromechanical devices like sensors, actuators, transducers, medical-applications [1-5]. The structure of PZT ceramics is a perovskite type structure described by the ABO_3 formula. Near the morpf/tropic phase boundary (MPB) the piezoelectric properties have maximum values [6]. In ABO_3 structure the Pb^{2+} ions occupying the A-site and the Ti^{4+} and Zr^{4+} ions occupying the B-site.

Preprints (www.preprints.org) | NOT PEER-REVIEWED | Posted: 22 May 2019 doi:10.20944/preprints201905.0265.v1

Depending on the radius ionic dopants can get in A or/and B position. The influence of different dopants like Sr^{2+}, Ba^{2+}, Sm^{3+}, La^{3+}, Nb^{5+}, etc. have been investigated for various specific properties required by the applications. We can modify the values of electro-physical parameters of the ceramics by dopping PZT system. We can obtain materials of increased or decreased ferroelectric-hardness by doping. Nb^{5+} can be considered as a donor dopant for PZT ceramics since it substitutes Zr^{4+}/ Ti^{4+} ions. Nb oxide is a good sintering aid for PZT compositions [7]. Sr^{2+} is an isovalent dopant for PZT ceramics substituting the Pb^{2+}. Sr^{2+} improved the dielectric permittivity (ε) and increases the electromechanical coupling coefficient (k_p) [8]. In the present work we have obtained and characterized the PZT ceramic doping by Nb^{5+} and Sr^{2+} which are used for piezo-motor application. In this paper, the PZT based ceramics with a composition described by the general formula $Pb_{(1-x)}Sr_x(Ti_{0.48}Zr_{0.52})_{(1-y)}Nb_yO_3$; x = 0.05 and y = 0.02 were prepared by conventional mixed-oxides techniques. The sintering temperature used was 1140 °C for 2 hours. The effects of dopants (Sr2+ and Nb5+) on phase constitution, on microstructure and on the dielectric and piezoelectric properties were determinate. The XRD data revealed that the PZT doped composition had tetragonal perovskite structure. The dielectric constant (ε_r) measured at 1 kHz is about 1100 and the dielectric loss factor (tanδ) is $16x10^{-3}$. The maximum value of the planar electromechanical coupling coefficient (kp) is 0.45. These parameters obtained for the PZT doped composition are useful for the development of piezo-motor applications. In the broad field of electric generated motion, the piezo motion gains increasingly more applications thanks to some outstanding technical qualities: fast response, high precision, high force or torque, long life, maintenance and lubricants free, compact dimensions, non-magnetic, UHV compatible [9-11]. The up mentioned properties seem to recommend the piezo motors for numerous applications in space industry. Although piezoelectric linear actuators are studied in detail and the research field offer many constructive solutions, the piezoelectric rotary engines appear to offer yet unexplored fields of application. Ultrasonic motors are very compact and can attain relatively small speeds combined with resolutions down to a few nanometers or better. Rotary motors feature high torques, especially at low rpm, [12-15]. The drawback to these piezomotors has traditionally been their difficulty of control. These problems were solved with the latest generation of ultrasonic motor controllers [16]. An autotuning circuit constantly keeps the oscillator frequency in the optimum range; and a fast processor automatically switches between gainsets, enabling the user to take full advantage of excellent velocity constancy, wide dynamic range, and the exceptional stability. The main aim of this paper was to present a new conceptual solution of a rotating ultrasonic piezo motor where the driven rotor is set in motion considering a friction coupling with a vibrating bending piezoceramic tube of a special structure [17,18]. A careful attention was payed to clear describing of the mooving mechanism by considering some simulation of a real laboratory demonstrator. Special analysis of the output performances were considered.

2. Materials and Methods

2.1. Material Composition

The piezoelectric material used in the design of the piezoelectric motor has been a modified lead zirconate titanate (PZT) with different dopants to enhance the desired piezoelectric properties. At room temperature, PZT compositions with Zr/Ti ~ 52/48 show high electromechanical properties close to the morphotropic phase boundary (MPB), [6, 19, 20]. The usage of Nb^{5+} as a donor dopant on the B side inhibits grain growth resulting in an increase of the density of the ceramic [20]. Furthermore, it is possible to improve the dielectric and piezoelectric charge coefficients through the doping of the Nb-doped PZT with Sr^{2+}, [21]. According to this phenomenon, the configuration chosen for the study of the material has been a PZT with a ratio Zr/Ti = 52/48 and using as dopants Sr^{2+} and Nb^{5+}, [22].

2.2. Manufacturing Procedure

The experimental research to characterize the modified PZT created focused on the composition described by the general formula: $Pb_{(1-x)}Sr_x(Ti_{0.48}Zr_{0.52})_{(1-y)}Nb_yO_3$ with x = 0.05 and y = 0.02. This formula corresponds with a group of compositions denoted as PZTSN. High purity oxides (purity

Preprints (www.preprints.org) | NOT PEER-REVIEWED | Posted: 22 May 2019 doi:10.20944/preprints201905.0265.v1

>99%) were used in the fabrication of the material and presented together with the provider: PbO (from Fluka), ZrO_2 (from Merck), TiO_2 (Aldrich), $SrCO_3$ (Carlo Erba) and Nb_2O_5 (Fluka).

The required quantity of each of the oxides was determined according to the formula and the mix homogenized in a Fritsch planetary type mill for a time of 10 hours using a water mixing environment. The resulting slurry was then dried at 80 °C in a box oven and uniaxially pressed in a stainless-steel die at a pressure of 50 MPa. Pellets were obtained with a measured density of 70% of the final theoretical density. The pellets were then calcinated in a high temperature Carbolite furnace at a temperature of 850 °C for 5 hours. Ball-milling of the resulting powder followed in a Fritsch planetary mill for another 10 hours in a media of H_2O. The resulting suspension was dried at 80 °C in the oven, mixed with a 5% aqueous solution of (APV) acting as a binder and then pressed uniaxially into 24 mm diameter and 2 mm thickness discs at 70 MPa. The formed samples were then sintered for 2 hours at 1140 °C. The sintering process was performed in a high temperature Carbolite furnace heating and cooling down at a rate of 5 °C/min.

The density of each of the samples was calculated through their weight and dimensions. The crystal phases of the sintered phases were analyzed using X-ray diffraction (Brucker AXS D8 Advance) with CuKα radiation and a Ni filter. The microstructure development was characterized using a scanning electron microscope (Workstation Auriga). All the sintered samples were polished and covered with a film of silver paste to act as electrodes.

The dielectrically properties were measured using an LCR meter (HAMEG type) at 1 kHz. The samples were poled in silicon oil at 1.6 kV/mm at 160 °C for 60 minutes and then allowed to cool down to room temperature while maintaining the applied electric field. The resulting piezoelectric properties were measured using an impedance analyzer 4294A (Agilent type).

2.3. Experimental Characterization

A single perovskite phase was detected on the samples sintered following the aforementioned procedure. The diffraction image for these samples is presented in Figure 1.

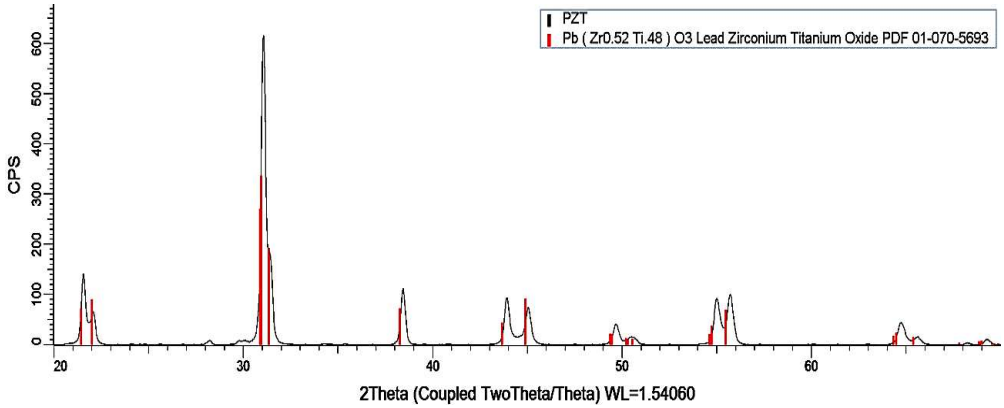

Figure 1. The diffraction image for samples sintered for 2 h at 1140°C.

A densification of the material is evident from the experimental measurements, which were correlated with SEM images. In Table 1 are presented the mean density measurements for 10 samples. The microstructure of one of the sintered samples that is obtained with the SEM microscope are illustrates in Figure 2.

Preprints (www.preprints.org) | NOT PEER-REVIEWED | Posted: 22 May 2019 doi:10.20944/preprints201905.0265.v1

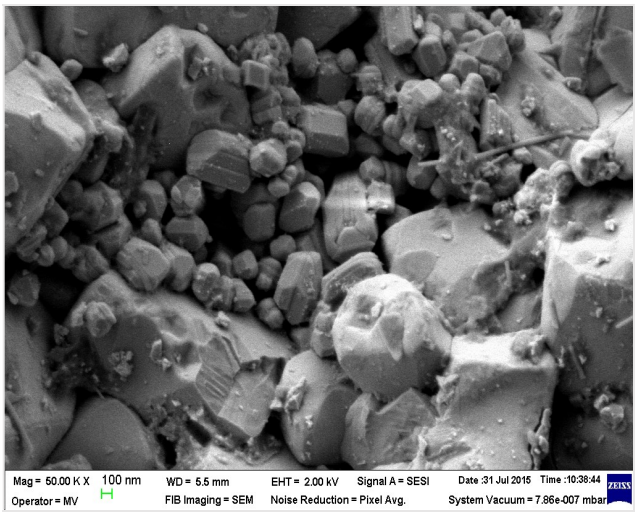

Figure 2. SEM micrographs of sintered PZTSN at 1140 °C for 2 hours.

Through the measurement of the capacitance as a function of temperature while exciting the piezoelectric samples at 1 kHz the Curie temperature was determined. The results of the average Curie temperature for the 10 samples together with the mean values of the relative permittivity, the loss angle tangent and the electromechanical coupling factor are presented in Table 1.

The sintering temperature has a direct effect on the dielectric constant ($\varepsilon_r = \varepsilon_{33}/\varepsilon_0$). The analysis of the resonance and antiresonance frequencies for the sintered samples allowed for the calculation of the electromechanical coupling factor (k_P).

Table 1. Physical and piezoelectrical properties for the sintered samples.

Density	Pa	Abs	Curie temperature	Electromechanical coupling factor (k_P)	Relative dielectric constant ($\varepsilon_r = \varepsilon_{33}/\varepsilon_0$)	Loss angle tangent (tanδ)
[g/cm^3]	[%]	[%]	[°C]	-	-	[x10^{-3}]
7.40	0.32	0.04	340	0.38 - 0.45	1100 ± 250	16

3. Motor Principle

3.1. Theoretical Considerations

The equations that describe the behavior of the used piezoelectric material in terms of the electromechanical coupling are presented in (1) or alternatively in (2) where indexes i, j = 1, 2,..., 6 and indexes m, k = 1, 2, 3 describe the material directions. Superscripts D, E and σ represent the determined values in constant electric displacement, constant electric field and constant elastic stress conditions. E and D are the electric field and displacement respectively, σ and ε the stress and strain tensors, ζ and β the permittivity constants in [F/m] and in [m/F] respectively, S the compliance matrix, d the piezoelectric deformation constants matrix in [m/V], and g the piezoelectric constants matrix in [m^2/N].

$$\begin{cases} \varepsilon_i = S_{ij}^E \sigma_j + d_{mi} E_m \\ D_m = d_{mi} \sigma_i + \zeta_{ij}^\sigma E_k \end{cases} \quad (1)$$

Preprints (www.preprints.org) | NOT PEER-REVIEWED | Posted: 22 May 2019 doi:10.20944/preprints201905.0265.v1

$$\begin{cases} \varepsilon_i = S_{ij}^D \sigma_j + g_{mi} D_m \\ E_i = g_{mi} \sigma_i + \beta_{ij}^\sigma D_k \end{cases} \quad (2)$$

These equations present the quasi-static approach to the behavior of the piezoelectric materials. Such hypothesis restricts the application of the model to cases in which the piezoelectric material operates well under its resonance frequency. Simple modal analysis of the piezoelectric cylinder demonstrates first two bending eigenmodes around 21 kHz as presented in Figure 3, [11] and the simulated nominal functioning regime of the motor resulting from Figure 10 denotes a frequency of about 1.67 kHz. This observation legitimates the quasi-static approach.

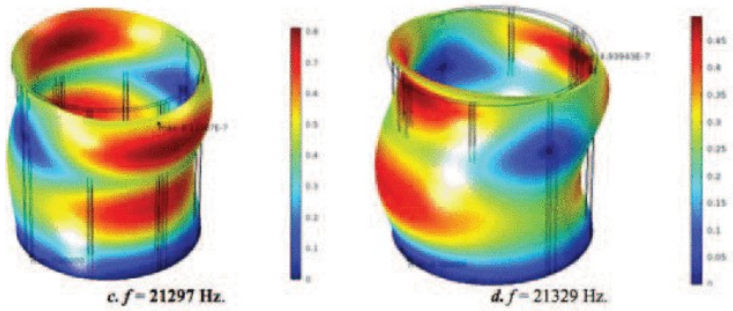

Figure 3. The first two bending eigenmodes of the PZT cylinder, [11].

A set of boundary conditions as presented in the following paragraphs will particularize the relations (1) and (2) for the conceptual design of the piezo-motor and allow integrate the relation between the external interactions and the model. These interactions between the modeled system and the external environment are either electric or mechanic. The electric interactions between the system and the external environment are an electric field, an electric potential or an electrical charge flow. In the analyzed case an electric potential was applied to the opposing electrodes of the piezoelectric cylinder. The piezoelectric cylinder was divided in 8 cylindrical sectors along the generatrix, as presented in Figure 4, each comprising an internal electrode surface (covered in a conducting plate) and an external electrode surface through which a voltage differential was applied. The actuation of the motor consisted in a sinusoidal actuation of the electrodes with a phase shift proportional to their position around the piezoelectric cylinder.

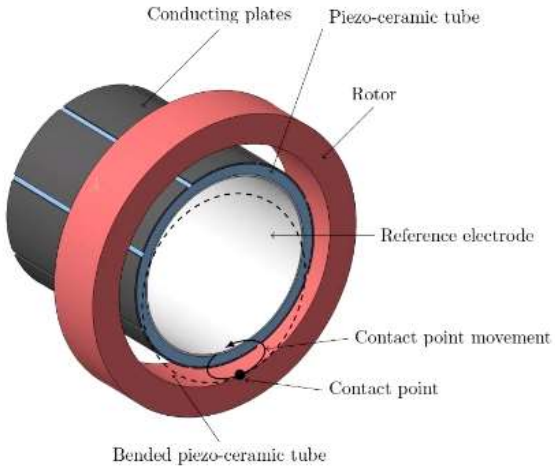

Figure 4. The conceptual design of the piezo-motor.

Preprints (www.preprints.org) | NOT PEER-REVIEWED | Posted: 22 May 2019 doi:10.20944/preprints201905.0265.v1

Two sets of mechanical boundary conditions (MBC) have been applied to the model, one for each of the studied cases. The idle case considered a model that had a degree of freedom: θ rotation of the rotor as presented in Figure 5. The cylinder was constrained displacement-wise in all directions in one of the ends while free in the other end to allow for bending deformation. The rotor was fixed in order to only allow rotation about its symmetry axis.

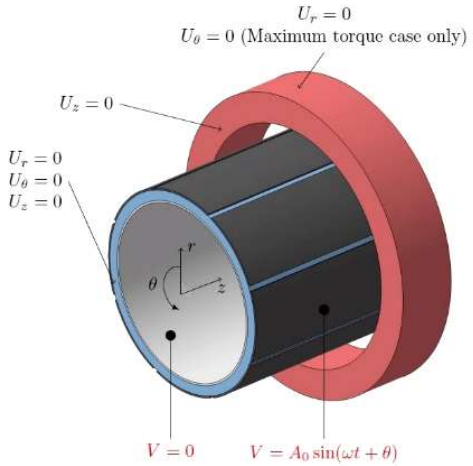

Figure 5. The boundary conditions for two functioning regimes.

MBC for the maximum torque case differ slightly from the idle case. An additional MBC is considered restricting the rotor rotation. This second simulation does not consider any degrees of freedom in the system. These boundary conditions are represented in Figure 5 as well as in Figure 6. The MBC are shown in black color for both simulation cases while the electrical boundary conditions (EBC) are shown in red.

3.2. Functioning Principle

The motor designed is based on the bending deformation of a piezoelectric tube. A piezoelectric tube is mounted inside a concentric rotor leaving a uniform and carefully calculated clearance. When the piezoelectric is actuated, the bending tube contacts the rotor with a pressure function of the applied tension on the electrodes of the piezoelectric tube. As the piezo-ceramic tube bends, the contact point between the cylinder and the rotor rotates about the motor axis dragging the rotor and generating the rotational motion in the motor. The contact force between the free end of the piezoelectric cylinder and the rotor, as a result of the movement of each contact point in an elliptical motion, generates a coulombian friction force and, as a result, a rotational motion of the rotor takes place. The maximum value of the torque is limited by the friction force:

$$M_r = F_f R_{rot} \leq \mu F_c R_{rot} \tag{3}$$

Where: M_r – torque; F_f – friction force; R_{rot} – inner radius of the rotor; μ - friction coefficient and F_c – contact force. The gap between the piezo-ceramic tube and the rotor must be carefully considered. A gap too large may result in no contact between the tube and the rotor or not enough contract pressure to produce motion in the rotor. On the other hand, too much pressure between the components leads to loss of efficiency. A tradeoff study of the gap dimension with respect to the resulting maximum friction force value as wel as to technological and functional implications will be welcome.

Preprints (www.preprints.org) | NOT PEER-REVIEWED | Posted: 22 May 2019 doi:10.20944/preprints201905.0265.v1

3.3. Numerical Simulation

The numerical simulations performed aimed to solve two different aspects of the motor functioning: firstly, to prove that the concept behaves in the desired manner; and secondly, to quantify the performance of the designed motor.

3.3.1. Finite element model

The model performed consisted of two major components, an inner tube composed of piezoelectric material and an outer rotor. Because of the geometry of the motor, 3D elements were used in the simulation with electromechanical coupling capabilities, as described in (1) and with physical and piezoelectric properties resulted and presented in Table 1. The model used in the rotor is adapted to the simulation needs, which are defined by its function which is to acquire the movement of the piezoelectric tube and transmit it to the motor shaft. Two approaches have been considered: non-deformable solid and a 3D elastic solid. The later has been used in the simulation because of the necessity to account for the local deformations in the contact zones with the piezoelectric tube. The piezoelectric tube presented different requirements in terms of the physical model required as it needed to describe the coupling between electric and elastic fields. Additionally, the model used also needed to be compatible with contact elements to transmit the motion to the rotor of the motor. The numerical element selected was a 3D 8-node cubic solid with both piezoelectric and contact capabilities as presented in Figure 7. The conducting plates covering the different segments of the piezoelectric cylinder were not modeled. It was considered that in order to demonstrate the functioning of the motor, the effect of the plates on the performance could be neglected without significantly affecting the results obtained.

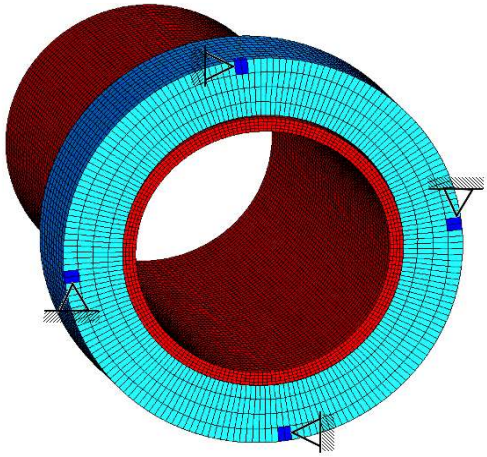

Figure 6. Supplementary MBC to block the rotational movement.

The simulation has been performed in two different cases: an idle-case, in which no external opposition torque was applied to the rotor, and a maximum torque case, in which the rotor was blocked (in terms of torque) to calculate the maximum torque that the motor could produce. The boundary conditions applied to the model are both mechanical and electric as shown in Figure 5. The piezoelectric cylinder was displacement-restricted at the base in all axes while the rotor was restricted to allow one degree of freedom (rotation around the symmetry axis) in the idle case. The model was further restricted mechanically in the maximum torque case blocking the rotational movement as presented in Figure 6.

Preprints (www.preprints.org) | NOT PEER-REVIEWED | Posted: 22 May 2019 doi:10.20944/preprints201905.0265.v1

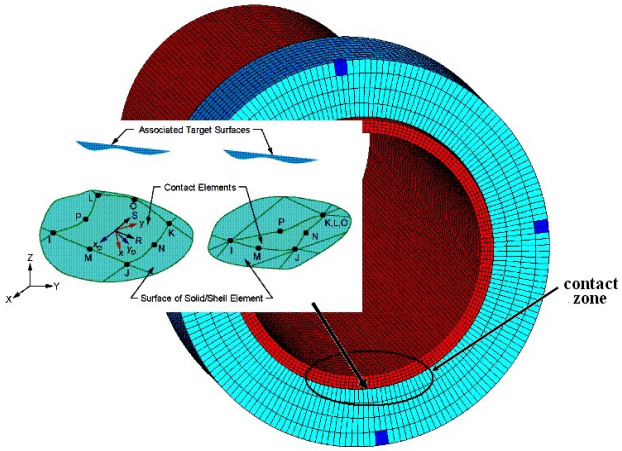

Figure 7. Contact region modeling.

The piezoelectric tube presented different requirements in terms of the physical model required as it needed to describe the coupling between electric and elastic fields. Additionally, the model used also needed to be compatible with contact elements to transmit the motion to the rotor of the motor. The numerical element selected was a 3D 8-node cubic solid with both piezoelectric and contact capabilities as presented in Figure 7. The conducting plates covering the different segments of the piezoelectric cylinder were not modeled. It was considered that in order to demonstrate the functioning of the motor, the effect of the plates on the performance could be neglected without significantly affecting the results obtained. The simulation has been performed in two different cases: an idle-case, in which no external opposition torque was applied to the rotor, and a maximum torque case, in which the rotor was blocked (in terms of torque) to calculate the maximum torque that the motor could produce. The boundary conditions applied to the model are both mechanical and electric as shown in Figure 5. The piezoelectric cylinder was displacement-restricted at the base in all axes while the rotor was restricted to allow one degree of freedom (rotation around the symmetry axis) in the idle case. The model was further restricted mechanically in the maximum torque case blocking the rotational movement as presented in Figure 6.

3.3.2. Numerical Results

The finite element calculations led to the results that are presented in this section. In the Figure 8 and Figure 9 is presented the electric field map and the z-displacement field map for the inner tube respectively to appreciate the extent of the electrodes placed around the tube and the electric excitation of the piezoelectric.

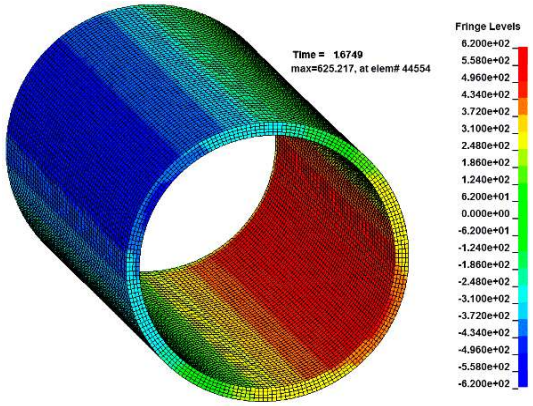

Figure 8. Electric field map.

Preprints (www.preprints.org) | NOT PEER-REVIEWED | Posted: 22 May 2019 doi:10.20944/preprints201905.0265.v1

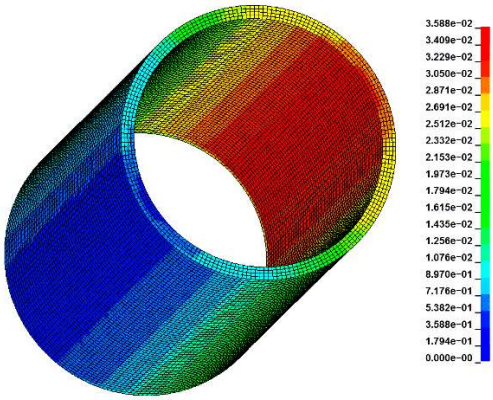

Figure 9. Displacements field map [mm].

In the Figure 7 is presented the configuration of the motor elements for the first case studied, in which no outside reaction torque was applied on the rotor. The rotor and the inner tube can be seen in blue and red elements. The darker blue groups of elements in the Figure 7 are the control points used to analyze the output torque of the motor, which is presented as a function of time in Figure 10.

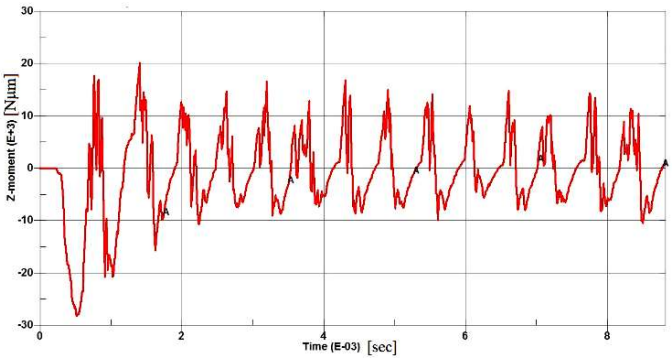

Figure 10. Torque - time variation of the rotor idle case.

The graphic of the output torque of the motor shows an initial peak consistent with the motor accelerating to its operating speed. After that the inertial effects minimize and the motor enters a steady state phase in which the net output for every cycle of the motor is zero. This result is consistent with the expected performance given that no friction is considered in the model apart for the friction developed in the contact between rotor and stator, which in this case dissipated no energy because the relative velocity between the two components is zero when the motor produces no output mechanical power. The case with fixed rotor was considered to determine the maximum torque that the motor could develop. Figure 6 depicts the configuration of the motor illustrating the elements that were considered blocked in the rotation direction of the rotor to determine the torque exerted by the motor. The rest of the boundary conditions applied to the idle-case simulation were maintained in this simulation. The graphic of the resulting torque produced by the motor is shown in Figure 11. The graphic shows a transitory response of the motor lasting for approximately one millisecond after which the motor torque output becomes steady with small oscillations about a value of 47 Nm (for a friction coefficient of 0.25).

Preprints (www.preprints.org) | NOT PEER-REVIEWED | Posted: 22 May 2019 doi:10.20944/preprints201905.0265.v1

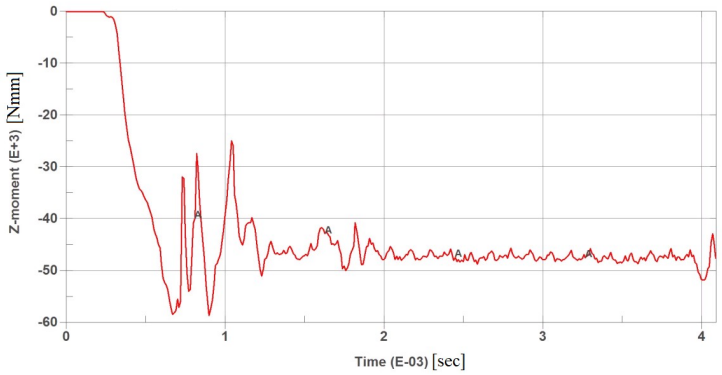

Figure 11. Torque - time variation of the rotor, maximum torque case.

In this case, the net torque output of the motor is no longer symmetric about zero moment. As the rotor is constrained and not allowed to freely rotate, a relative velocity appears at the contact points between the piezoelectric tube and the rotor which results in the friction force between the two components producing a work. Hence, the motor produces torque in this simulation. On the other hand, as the rotor is not allowed to rotate, the power output of the motor is, like in the idle-case, zero.

4. Conclusions

A solid solution of piezoelectric ceramic was synthesized according to the general formula $Pb_{(1-x)}Sr_x(Ti_{0.48}Zr_{0.52})_{(1-y)}Nb_yO_3$ with x = 0.05 and y = 0.02, using wet ceramic processing technology and using an oxide mix as prime material. The Zr/Ti ratio was chosen near the morphotropic phase boundary of the PZT system in the studied composition. The developed ceramic sintered at 1140 °C for 2 hours allowing for good dielectric and piezoelectric properties such as, the dielectric constant (ε_r) measured at 1 kHz is about 1100 and the dielectric loss factor (tanδ) is $16x10^{-3}$. Also, the maximum value of the planar electromechanical coupling coefficient (kp) is 0.45. Such properties recommended the developed material composition to be used in piezo-motors with surface wave "actuation". The simulation demonstrates good output parameters of the piezo-motors especially in torque values and stability terms. The transitory response of the piezo-motors lasting for approximately one millisecond to the steady state regime demonstrates good terms of performance. The friction coefficient can be a leading manner to improve the performances. A future analysis of the thermal influence of the friction in time functioning terms will be welcomed. The designed piezo-motors was proven to work and for simulated case, demonstrates that for rotational velocities around 27 rpm could develop a torque of about 47 Nm.

Author Contributions: Authors have equally contributed to this work.

Acknowledgments: This work was supported by a grant of the Romanian Space Agency ROSA, Program for research – Space Technology and Advanced Research – STAR, Project Number 88/2013.

Conflicts of Interest: The authors declare no conflict of interest.

References

1. Newnham R.E., Ruschau G.R., "Smart electroceramics", J. Am. Ceram. Soc., 74 (1991) pp.463-480.

2. Cross L.E., "Review: Ferroelectric materials for electromechanical transducer applications", Mater. Chem. Phys., 43 (1996), pp. 108-115.

3. Setter N., Waser R., "Electroceramic materials", Acta Mater., 48 (2000), pp. 151-178.

4. Wallaschek J., "Piezoelectric Ultrasonic Motors", J. Intell. Mat. Syst. Structures, 6 (1995), pp. 71-73.

5. Tressler J.F., Alkoy S., Newnham R.E., "Piezoelectric sensors and sensor materials", J. Electroceramics, 2:4 (1998), pp. 257-272.

6. Jaffe B., Cook W.R., Jaffe H., "Piezoelectric Ceramics", London New York, Academic Press, 1971.

7. Mirzaei A., Banyani M., Torkian S., "Effect of Nb doping on sintering and dielectric properties of PZT ceramics", Processing and Application of Ceramics, 10[3] (2016), pp. 175-182.

8. Kalem V., Çam I., Timuçin M., "Dielectric and piezoelectric properties of PZT ceramics doped with strontium and lanthanum", Ceramics International, 37 (2011), pp. 1265-1275.

9. Mircea Ignat, George Zarnescu, Lucian Pîslaru–Dănescu, „Piezoelectric Micromotor with Coaxial Cylindrical Convertor", Proceedings of the International Aegean Conference on Electrical Machines and Power Electronics ACEMP'07 2007, 10-12 Sept. 2007, Bodrum, Turkey, DOI: 10.1109/ACEMP.2007.4510490, pp. 93-96.

10. A.M. Morega, G. Robello, M. Morega, and L. Pîslaru-Dănescu, "Numerical Study of the Stator Motion in a Piezoelectric Ultrasonic Motor", Proceedings of the 9th International Symposium on Advanced Topics in Electrical Engineering ATEE 2015, 7-9 May 2015, Bucharest, Romania, DOI: 10.1109/ATEE.2015.7133878, pp. 609–613.

11. Morega A.M., Morega M., Pîslaru-Dănescu L., "Piezoelectric Ultrasonic Traveling Wave Motor", Proceedings of the 2016 INTERNATIONAL CONFERENCE ON APPLIED AND THEORETICAL ELECTRICITY (ICATE), 06-08 Oct. 2016, Craiova, ROMANIA, DOI: 10.1109/ICATE.2016.7754661.

12. Junkao Liu, Shengjun Shi, Weishan Chen, Huijun Dong, "Design and Primitive Study of a Cylindrical Traveling Wave Ultrasonic Motor Using Outer Excitation", Proceedings of the 2010 International Symposium on Optomechatronic Technologies, 25-27 Oct. 2010, Toronto, ON, Canada, DOI: 10.1109/ISOT.2010.5687384.

13. Karl Spanner and Burhanettin Koc, "Piezoelectric Motor Using In-Plane Orthogonal Resonance Modes of an Octagonal Plate", Actuators 2018, 7, 2; doi:10.3390/act7010002, pp. 1-14.

14. Safakcan Tuncdemir, Seyit O. Ural, Burhanettin Koc and Kenji Uchino, "Design of Translation Rotary Ultrasonic Motor with Slanted Piezoelectric Ceramics", Japanese Journal of Applied Physics 50 (2011) 027301, DOI: 10.1143/JJAP.50.027301, pp. 1-8.

15. Yingxiang Liu, Weishan Chen, Peilian Feng, Junkao Liu, "A rotary piezoelectric motor using bending vibrators", Sensors and Actuators A: Physical, 196 (2013), pp. 48– 54.

16. Joel Shields, "Asynchronous Control of a Prototype Inchworm Actuator: Control Design and Test Results", Actuators 2019, 8, 20; doi:10.3390/act8010020, pp. 1-21.

17. Nesbitt W. Hagood and Andrew J. McFarland, "Modeling of a Piezoelectric Rotary Ultrasonic Motor", IEEE Transactions on Ultrasonics, Ferroelectrics, and Frequency Control, Volume: 42, Issue: 2 , March 1995, DOI: 10.1109/58.365235, pp. 210-224.

18. Elena Teidelt, Valentin L. Popov, Ha X. Nguyen, Sergej Fatikow, "Dynamic Tangential Contacts: Numerical Description of Nano-Positioning Devices", Proceedings of the 2014 International Conference on Manipulation, Manufacturing and Measurement on the Nanoscale (3M-NANO), 27-31 Oct. 2014, Taipei, Taiwan, DOI: 10.1109/3M-NANO.2014.7057315, pp 280-284.

19. Chiang S.S., Nishioka M., Fulrath R.M., Pask J.A., "Effect of processing on microstructure and properties of PZT ceramics", Am. Ceram. Soc. Bull., 60 (1981), pp. 484–489.

20. Wu L., Wei C.C., Wu T.S., Liu H.C., "Piezoelectric properties of modified PZT ceramics", J. Phys. C: Solid State Phys., 16 (1983), pp. 2813–2821.

21. Kozielski L., Adamczyk M., Erhart J., "Application testing of Sr doping effect of PZT ceramics on the piezoelectric transformer gain and efficiency proposed for MEMS actuators driving", Journal of Electroceramics, 29 (2012), pp. 133-138.

22. Chowdhury P.R., Deshpande S.B., "Effect of dopants on the microstructure and lattice parameters of lead zirconate–titanate ceramics", J. Mater. Sci., 22 (1987), pp. 2209–2215.